Molecular Crystals and Liquid Crystals Incorporating Nonlinear Optics

Publication details, including instructions for authors and subscription information:
http://www.tandfonline.com/loi/gmcl17

Transitions to Liquid Crystalline Phases in a Semifluorinated Alkane

C. Viney [a b], T. P. Russell [a], L. E. Depero [a] & R. J. Twieg [a]

[a] IBM Almaden Research Center, San Jose, California, 95120-6099, USA

[b] Department of Materials Science and Engineering, University of Washington, Seattle, Washington, 98195, USA

Version of record first published: 04 Oct 2006.

To cite this article: C. Viney , T. P. Russell , L. E. Depero & R. J. Twieg (1989): Transitions to Liquid Crystalline Phases in a Semifluorinated Alkane, Molecular Crystals and Liquid Crystals Incorporating Nonlinear Optics, 168:1, 63-82

To link to this article: http://dx.doi.org/10.1080/00268948908045960

Mol. Cryst. Liq. Cryst., 1989, Vol. 168, pp. 63–82
Reprints available directly from the publisher
Photocopying permitted by license only

Printed in the United States of America

Transitions to Liquid Crystalline Phases in a Semifluorinated Alkane

C. VINEY, † T. P. RUSSELL, L. E. DEPERO and R. J. TWIEG
IBM Almaden Research Center, San Jose, California 95120-6099, USA

(*Received June 1, 1988*)

Perfluorodecyl decane, $F(CF_2)_{10}(CH_2)_{10}H$, is shown to undergo a liquid crystal–liquid crystal transition above room temperature. The accompanying reversible structural reorganization is observed by transmitted polarized light microscopy, small angle x-ray scattering and wide angle x-ray diffraction. Both liquid crystalline phases have a layered structure; within the layers the molecules are interdigitated, tilted relative to the layer normal, and packed in a pseudo-hexagonal fashion. The transformation between the structures is achieved by a change in molecular tilt, together with a change in the extent to which the molecules are interdigitated within each layer.

Keywords: Tilted smectic, layered, interdigitated, pseudo-hexagonal, semifluorinated alkane, reversible transition

INTRODUCTION

A reversible transition between highly ordered phases has been described previously[1,2] for materials of the general formula $F(CF_2)_n(CH_2)_mH$. Information about the structure of these phases, and about the transition, was obtained from small- and wide-angle x-ray diffraction, Raman scattering, and differential scanning calorimetry (DSC). This led to the conclusion that the room temperature phase is crystalline, while the molecules have considerable freedom to rotate about their long axes at temperatures above this transition. The possibility exists, therefore, that this higher temperature phase might be a rotator phase[2] or a highly ordered liquid crystal such as smectic B or E.[3,4] Both phases were found to have a layered structure.

A subsequent study,[5] involving optical microscopy, has shown that the high temperature ordered phase in one of these compounds (perfluorodecyl decane, also denoted $F(CF_2)_{10}(CH_2)_{10}H$ or simply F10H10) is a smectic B liquid crystal. No information on the structure of the room temperature solid phase was reported in this work.

In the present paper, we discuss detailed results obtained from optical microscopy, DSC, and small- and wide-angle diffraction studies of F10H10. We identify

†Present address: Department of Materials Science and Engineering, University of Washington, Seattle, Washington 98195, USA.

and characterize *tilted* smectic liquid crystalline phases, both above the transition and at room temperature. Further, we propose a mechanism for the transition between these phases on heating and cooling.

In anticipation of these results, we shall in future write LC1 and LC2 to denote the phases, with the shorthand LC2 referring to the phase that is stable at lower temperatures. We shall use the term "transition temperature" to denote the temperature above which LC1 is formed on heating and below which LC2 forms on cooling. The term "melting" will refer only to the formation of an isotropic phase from LC1 on heating.

SYNTHESIS OF MATERIAL

The semifluorinated alkane F10H10 was prepared by conventional means involving addition of perfluorodecyl iodide to 1-decene and subsequent dehalogenation of the iodide-containing intermediate with zinc in ethanolic HC1. The intermediate and product were easily purified by simple distillation and the F10H10 was determined to be > 99% pure by gas chromatographic analysis.

F10H10I, or 1,1,1,2,2,3,3,4,4,5,5,6,6,7,7,8,8,9,9,10,10-undodecafluoro-12-iodoicosane

In a 100 ml round bottom flask with stirbar, reflux condenser and nitrogen inlet was placed perfluorodecyl iodide (12.92 g, 20.0 mmol) and 1-decene (2.80 g, 20.0 mmol). This mixture was warmed with stirring in an 80°C oil bath and AIBN (30 mg) was added. After 15 minutes the bath temperature was raised to 90°C and additional AIBN (30 mg) was added. After 15 minutes the reaction mixture was cooled to a waxy solid and fractionated by kugelrohr distillation. The center cut, boiling in the range 105°C–110°C at 90 μ and totalling 12.91 g (82%), was retained.

F10H10, or 1,1,1,2,2,3,3,4,4,5,5,6,6,7,7,8,8,9,9,10,10-undodecafluoroicosane

In a 250 ml 3-neck round bottom flask equipped with stir bar, gas inlet tube, condenser and bubbler was placed F10H10I (3.14 g, 4.0 mmol) and ethanol (100 ml). The slurry was warmed to a gentle reflux, a slow stream of HCl gas was admitted and zinc powder (1.05 g, 16.0 mmol) was added in small portions over the next 20 minutes. After this time gas chromatography indicated the absence of any starting iodide and the reaction mixture was cooled and transferred to a separatory funnel with hexane and water. The phases were separated and the organic phase was washed with saturated sodium bicarbonate, dried ($MgSO_4$) and filtered through a pad of silica gel. After concentration by rotary evaporation the material was fractionated by kugelrohr distillation. A center cut boiling at 85°C and 250 μ was retained, precipitated from a mixture of acetone and ethanol and isolated by suction filtration to give 2.33 g (88%) of F10H10.

EXPERIMENTAL

Thermal analysis

Thermal analysis was performed on a DuPont 1090 system. Specimens with a mass of 10 mg (approx.) were scanned at 10°C/minute, while being maintained in an

atmosphere of dry nitrogen. A typical thermal history consisted of the following sequence: as-synthesized material was heated (scan 1) to approximately 10°C above the endotherm associated with melting to an isotropic phase (as confirmed by optical microscopy). The specimen was then cooled (scan 2) to room temperature at the same rate, and this heating/cooling cycle was then repeated immediately (scans 3 and 4).

Optical Microscopy

Microscopy was performed on specimens held between a conventional rectangular glass microscope slide and cover slip, using a Carl Zeiss (Jena) Amplival polarizing microscope. Microstructures (textures) were observed at elevated temperatures with the help of a Mettler FP52 hotstage and FP5 controller, which provided for a variety of heating/cooling rates as well as for viewing under isothermal conditions.

Small angle x-ray scattering

Small-angle x-ray scattering (SAXS) data were collected on beamline I-4 at the Stanford Synchrotron Radiation Laboratory. The white radiation from a bending magnet impinged on a 0.5 m float glass mirror coated with platinum. The mirror, tilted at 17 mrad with respect to the incident beam, was bent to focus the beam in the vertical direction. The beam was then focused horizontally and monochromated by a bent Si (111) crystal. Four sets of slits eliminated unwanted parasitic radiation prior to impingement on the specimen. Monitors before and after the specimen continuously provided a measure of the incident beam flux and the attenuation factor of the specimen. At the sample, the beam was approximately 0.75 mm in diameter. The detector, separated by an evacuated flight path of *ca* 50 cm, was a reticon selfscanning photodiode array cooled to *ca* − 80°C to reduce dark current and to maximize the dynamic range. Scattering profiles were collected and stored on a hard disk via CAMAC electronics for later use. Temperature control of the specimen was achieved by use of a Mettler FP85 hotstage which was placed in the scattering geometry. The 2 mm holes in the hot stage were suitable for allowing the incident and scattered x-rays to pass unhindered.

Wide angle x-ray diffraction

Wide-angle x-ray diffraction (WAXD) patterns were recorded in transmission on a flat plate camera under vacuum (Warhus Co.). Specimens were held in Lindemann glass capillaries having an internal diameter of 1mm. Electrical power input to the heater was regulated by an Omega temperature controller, which, in the range of interest, maintained the temperature to within ± 1°C. The specimen-to-film distance was 45.62 mm. Recorded diffraction patterns were digitized by means of a Cohu 5200 video camera (newvicon tube) and Imaging Technology 151 Image Processor (driven by a PC/AT), and then transferred to a host computer for obtaining diametrical scans.

RESULTS AND DISCUSSION

Results from DSC runs

Typical DSC traces for heating (scans 1 and 3) and cooling (scans 2 and 4) are shown in Figure 1. Quantitative enthalpy data and peak positions obtained from the original traces are given in Table I.

The traces show 2 endotherms on heating, and a single exotherm on cooling. Optical microscopy (see below) confirms that the endotherms correspond to the transitions LC2 → LC1 and LC1 → isotropic. The enthalpy associated with the cooling exotherm in scans 2 or 4 is less than the sum of the enthalpies of the two heating endotherms in scans 1 or 3. In the absence of any exotherms to indicate "recrystallization" in scans 1 or 3, we therefore deduce that the missing enthalpy is released as a slowly varying function of temperature and time on cooling, and is therefore not detected. This in turn suggests that the formation of LC2 from LC1 is dominated by kinetic factors. Data obtained from scan 1 (where the enthalpy for LC2 → LC1 is significantly larger than in scan 3) support this conclusion, since the as-synthesized material is obtained by precipitation from solution and can therefore be expected to attain greater structural perfection than a sample cooled from the melt.

We note that the enthalpy of the endotherm LC1 → isotropic is about three times that typical[6] of melting transitions involving smectic mesophases. However, such a direct comparison of values may be uninformative in the sense that the reviewed literature data for smectics pertains to systems based on aromatic monomers.

Optical Microscopy of LC1

At room temperature, as-synthesized material can be made to flow between a glass microscope slide and cover slip, if pressure is applied firmly to the latter with a dissecting needle. This suggests that the material is less than perfectly crystalline.

TABLE I

Quantitative DSC Data Obtained from Traces Shown in Figure 1

Scan Number	$T_{LC2\text{-}LC1}$ °C	$\Delta H_{LC2\text{-}LC1}$ J/gram (kJ/mole)	$T_{LC1\text{-}iso}$ °C	$\Delta H_{LC1\text{-}iso}$ J/gram (kJ/mole)	$\Sigma \Delta H$ J/gram (kJ/mole)
1 (first heating)	46.9	11.0 (7.3)	63.3	39.7 (26.2)	50.7 (33.5)
2 (first cooling)			59.9	−41.7 (−27.5)	−41.7 (−27.5)
3 (second heating)	37.3	3.3 (2.2)	63.5	40.5 (26.7)	43.8 (28.9)
4 (second cooling)			59.7	−41.9 (−27.7)	−41.9 (−27.7)

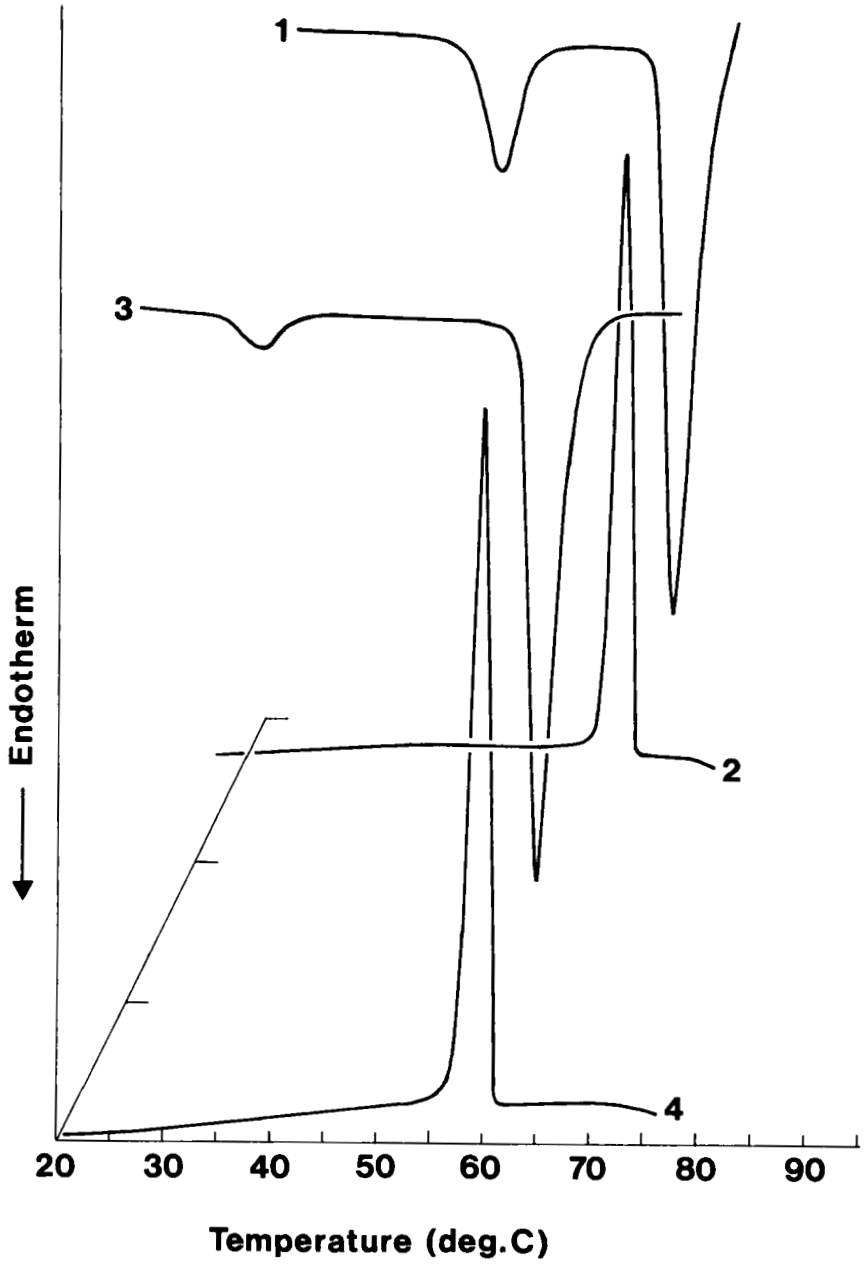

FIGURE 1 Typical sequence of DSC traces obtained from F10H10; specimens scanned at 10°C/min. in an atmosphere of dry nitrogen. (a) scan 1, heating; (b) scan 2, cooling; (c) scan 3, heating; (d) scan 4, cooling.

As-synthesized material heated at 2°C/min. becomes markedly more plastic above *ca* 45°C, and melts at 62.1°C to give a clear isotropic fluid. Specimens then cooled at 2°C/min. from 70°C form a distinctive liquid crystalline phase below 59.2°C (Figure 2a). The textures of this phase are characteristic of a tilted smectic B[7] or a smectic G or J[6] liquid crystal. These three terms do not all refer to different phases; they are synonymous with a structure based on a C-centered monoclinic unit cell, in which the molecules are packed in pseudo-hexagonal fashion. In planes intersecting the structure normal to the tilt direction, the packing gives the appearance of being truly hexagonal. The ambiguity of naming convention arose as a consequence of the historical order in which different research groups independently identified this structure as constituting a new phase. The terms "smectic G" and "smectic J" are now preferred, with "G" and "J" respectively indicating a tilt of the molecules towards the midpoint of a side or towards a vertex of the pseudo-hexagonal basal net.[6]

Specific features of the textures which justify classification of LC1 as smectic G or J are the following:

1. The characteristic mosaic texture, such as that shown in Figure 2a, does not contain any optically isotropic grains: all the domains show 4 intensity maxima and 4 extinction orientations when rotated through 360° between crossed polars. Thus there is no evidence of the molecular homeotropy that would be expected in at least some domains of a non-tilted phase.
2. The birefringence of individual domains increases slightly on cooling: the interference color may move discernibly up Newton's scale as the temperature decreases below the transition at which the domains were formed. Such an observation can be interpreted in terms of a small increase in molecular tilt. If the optical anisotropy of the domains is sufficiently high, the increase in tilt need not necessarily lead to a change in smectic layer spacing that is detectable within the accuracy limits of our SAXS data.
3. The individual domains all have an anisotropic shape, and they all have an anisotropic growth rate when forming from the isotropic melt. A non-tilted structure would lead to the presence of a significant number of equi-axed grains/domains.
4. Conoscopic imaging of low birefringence domains (*i.e.* domains in which the molecular alignment will be most nearly homeotropic) yields an interference figure of the form shown in Figure 3, indicating biaxial optical properties. Angular calibration of the field of view can be achieved by observing the position of the first order maxima obtained when the specimen is replaced by various diffraction gratings of known spacing. We can then use the separation of the melatopes in the interference figure of F10H10 to estimate the (small) angle by which the molecular long axes are tilted from the layer normal. The tilt angle is estimated as being approx. 5° at 50°C, before the structure transforms to LC2 as described below.
5. Shearing the cover slip across the specimen causes the microstructure to break up along the boundaries between domains. In smectic B (untilted), such deformation would normally lead to shear flow of the material. Firm downward pressure, exerted on the cover slip with a dissecting needle, does however lead to observable flow.

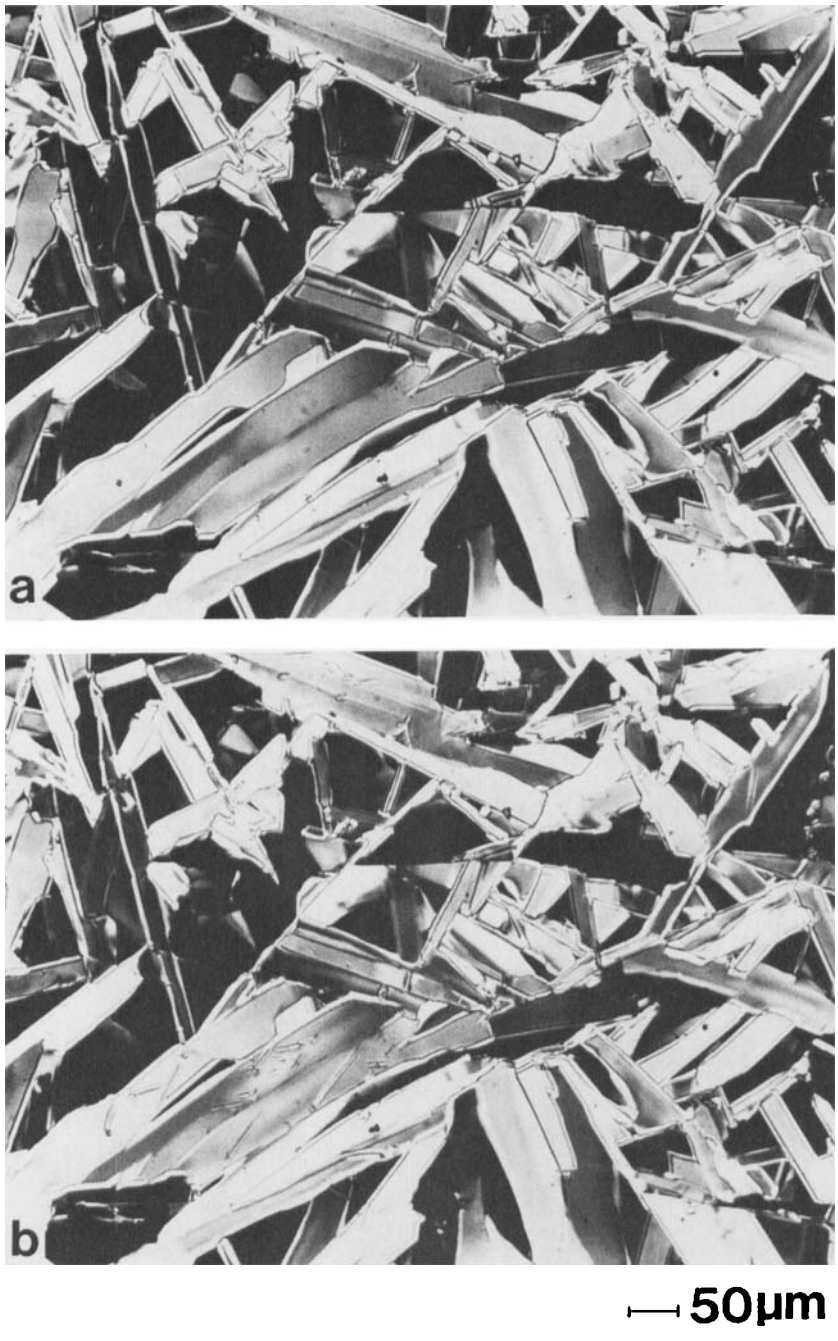

FIGURE 2 Optical textures of F10H10 as observed in transmission between crossed polars: (a) specimen at 55°C after cooling at 2°C/minute from the isotropic melt; (b) specimen after further cooling at this rate to 45°C; (c) specimen after further cooling at this rate to 38°C; (d) specimen after further cooling at this rate to 30°C; (e) specimen re-heated at 2°C/minute to 40°C; (f) specimen after further heating at this rate to 50°C.

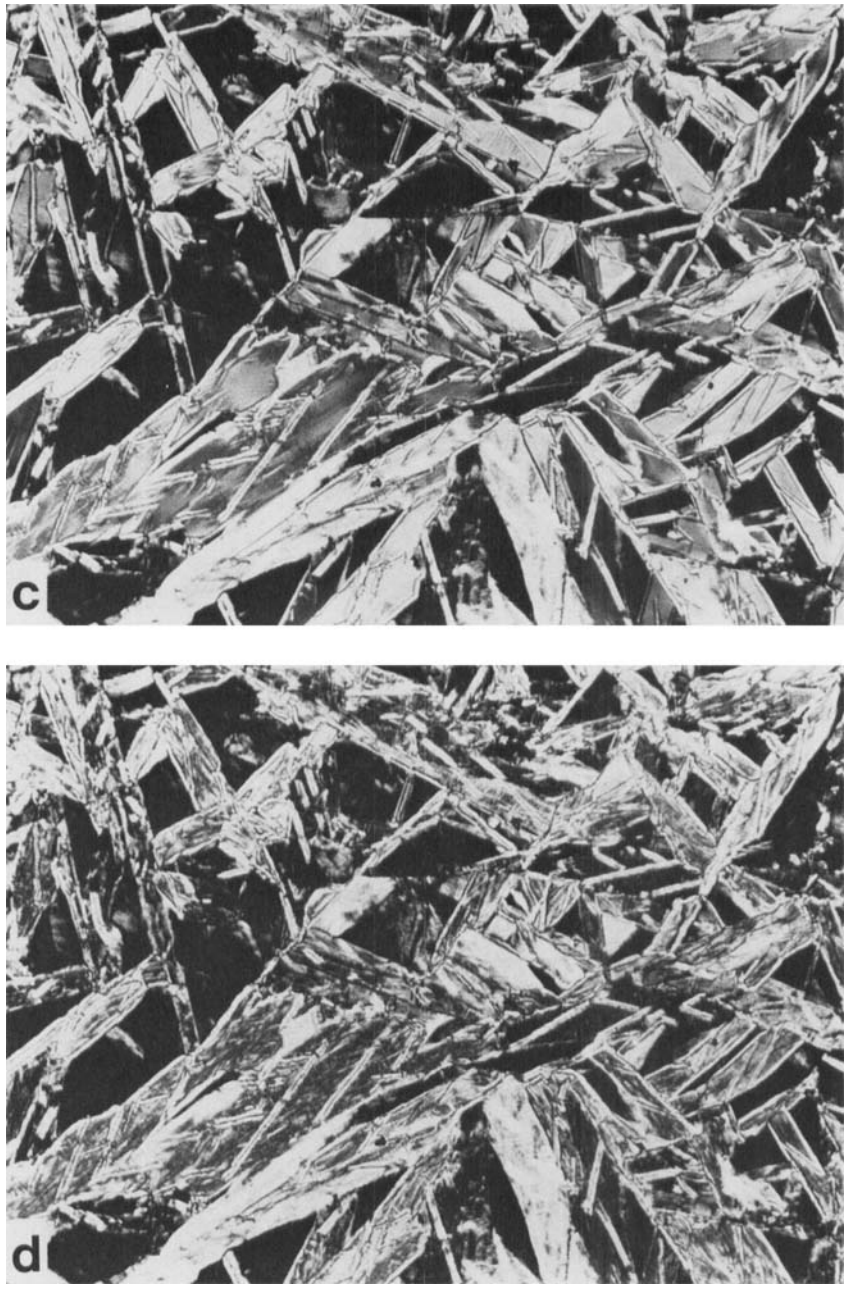

FIGURE 2 (*continued*)

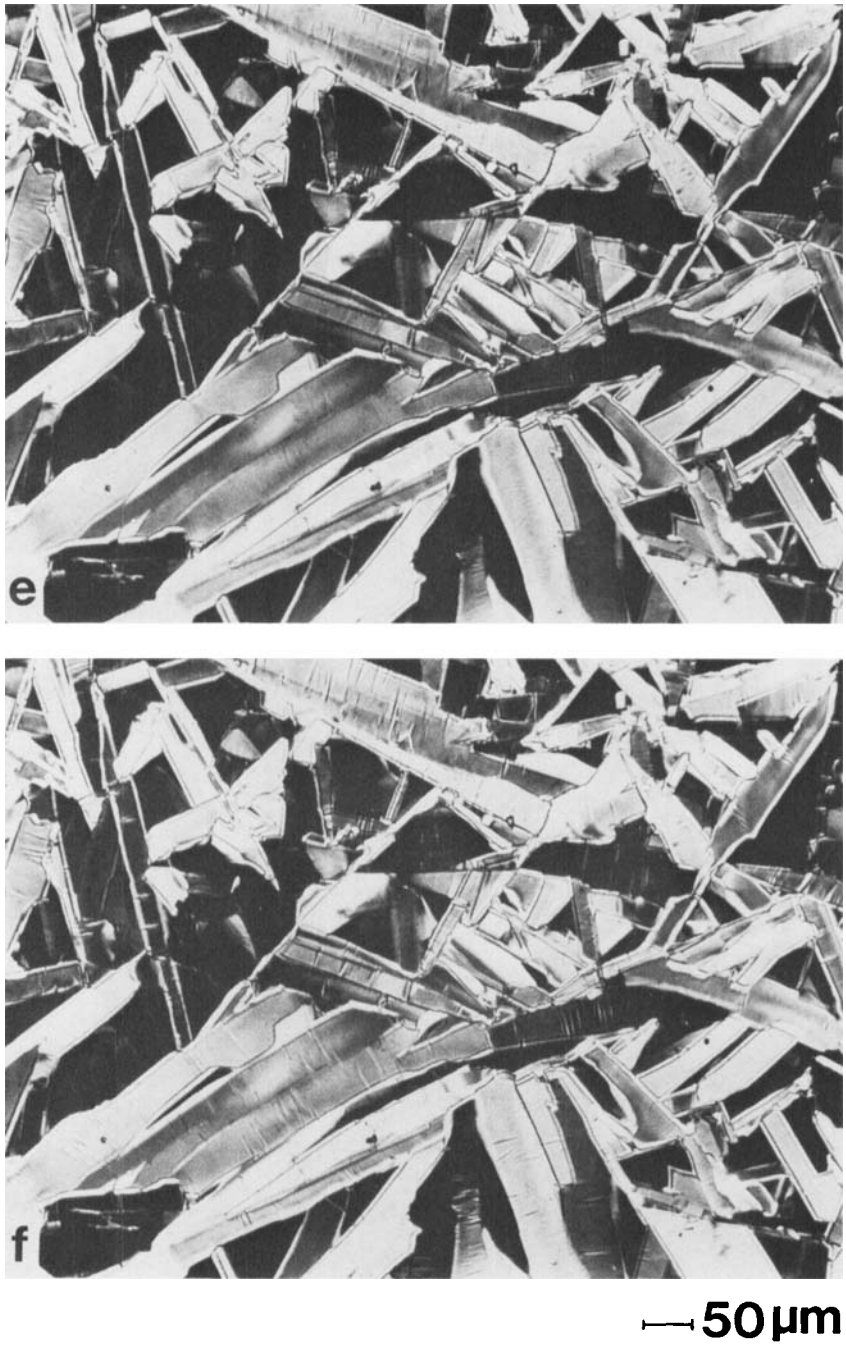

FIGURE 2 (*continued*)

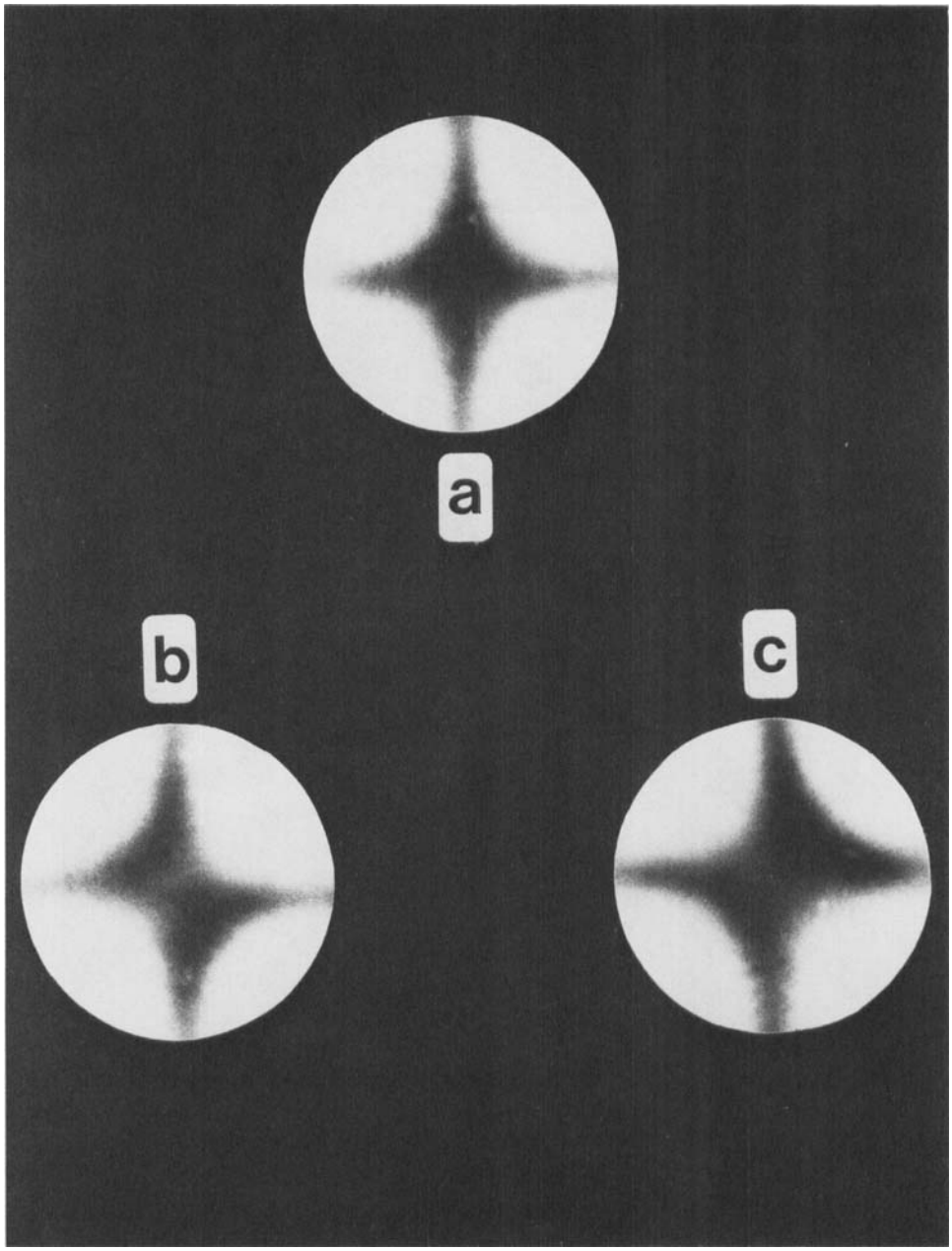

FIGURE 3 Conoscopic images (interference figures) obtained from a single low-birefringence domain of F10H10 at 55°C. The specimen previously had been cooled from the isotropic melt. (a) domain in extinction orientation between crossed polars; (b) specimen rotated 45° anticlockwise from orientation in (a); (c) specimen rotated 45° clockwise from orientation in (a). The behavior of the isogyres in these images is typical of that observed in the centered acute bisectrix figure of a specimen having a small optic axial angle.

Optical Microscopy of LC2

The mosaic texture of LC1 subsequently undergoes a transformation to a fine-textured phase (LC2) on further cooling. The transformation can be achieved isothermally at any temperature below about 55°C, though the temperature markedly affects the timescale over which the transformation occurs: several hours are required at 55°C, but the process takes only a few seconds at room temperature. The scale of the new texture depends strongly on the cooling rate, becoming finer as the cooling rate increases.

The individual domains in LC2 have a well-defined orientation of habit relative to that of the parent domains (Figures 2b–2d). The scale of the new microstructure becomes finer with decreasing transformation temperature, and is never coarse enough to enable positive recognition of a definitive liquid crystalline texture. However, in the light of previous work on related materials[1,2] below their transition temperature, we can anticipate that the structure will again consist of layers of tilted molecules.

There are 2 orientations in which one might expect LC2 to develop from LC1. Note that, if LC1 had the conventional hexagonal smectic B structure, one would instead anticipate 6 possible orientations of LC2 to develop from any one LC1 domain.

Figure 4 shows how a tilted smectic B-like phase, such as smectic G or J, might transform to another tilted phase. According to this model, the molecular tilt in LC2 could consist of a successive combination of the tilts that characterize smectic G and smectic J, with one component on its own being sufficient to characterize the LC1 phase. While tilted smectic phases of such mixed character have not been described previously, there is no symmetry-related reason why they should not exist. We anticipate that a tilt towards the midpoint of a side of the basal net (smectic G component) would accompany cooling of LC1, and that a tilt component towards a vertex (smectic J component) would be associated with the transition from monoclinic LC1 to triclinic LC2. This is because the latter component allows molecules to slip past each other in close-packed planes, and is therefore likely to be favored at lower temperatures.

On reheating, the microstructure undergoes further changes, as shown in Figures 2e–2f. The outlines of the original domains of LC1 (as formed during the most recent cooling from the isotropic state) are still preserved, but the domains of LC2 are replaced by striations running normal to the length of the original LC1 domains. The sequence of tilts suggested above can be reversed for the transition LC2 to LC1 on heating, and would explain why only a single orientation of LC1 reappears above the transition.

X-ray Diffraction from LC1

Results from SAXS, obtained at different temperatures on heating a sample of F10H10, are shown in Figure 5. Figure 6 shows WAXD data for two temperatures—one above the transition and the other below it. All the *d*-spacings measured from the original diffraction data are collected in Table II.

Looking at the SAXS data, we see that the transition from LC2 to LC1 occurred

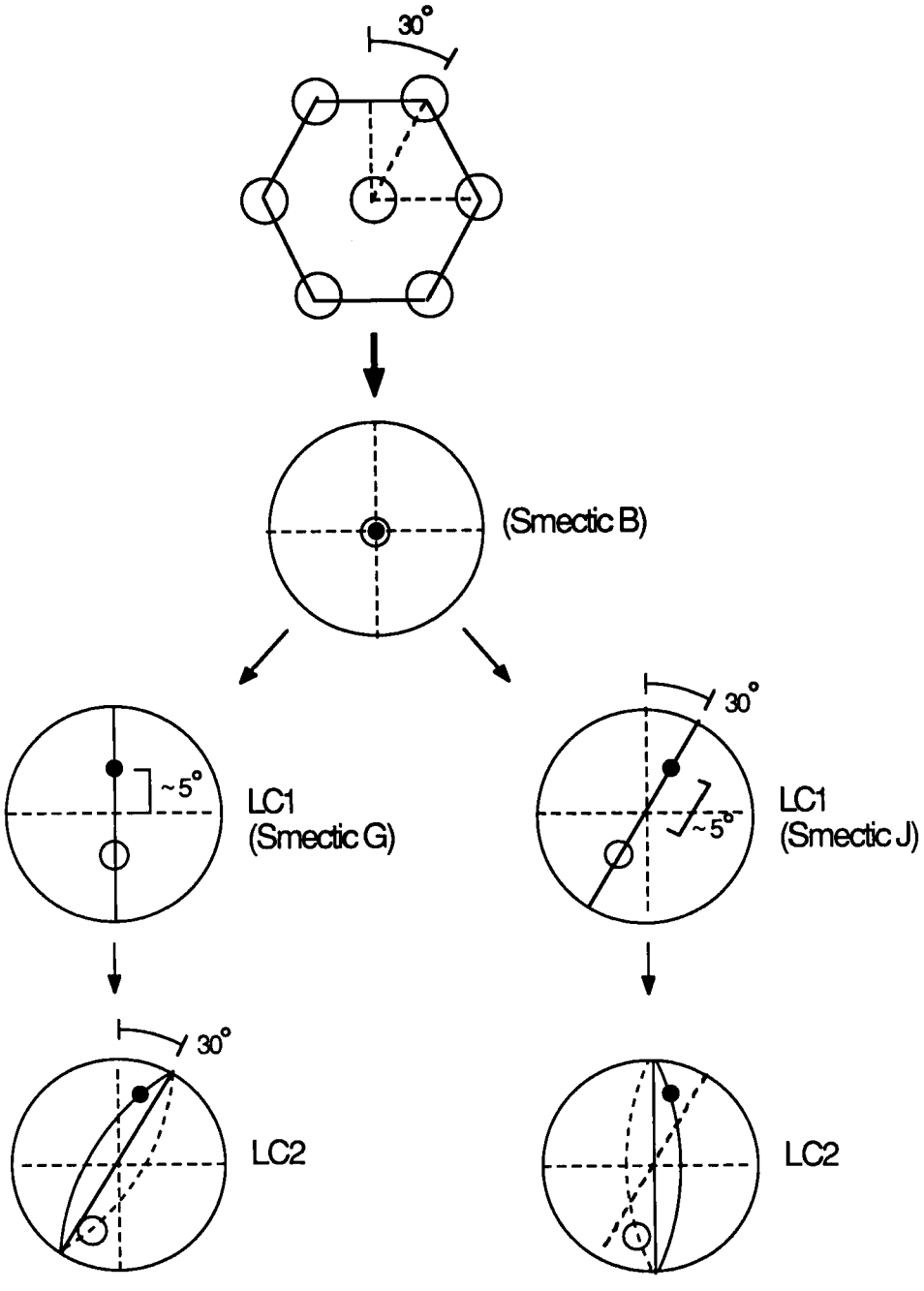

FIGURE 4 Relationship between the possible structures of LC1 and the corresponding structures of LC2. (For the sake of clarity, only one of the two symmetry-related structures of LC2 is shown in each case.) The relationship between LC1 and the conventional hexagonal smectic B structure is also shown. Molecular tilts (exaggerated) are represented on a stereographic projection that is centered on the normal to the smectic layers. Filled and open circles indicate the top and bottom ends of molecules respectively. Tilts have been exaggerated, to facilitate their representation on the diagram.

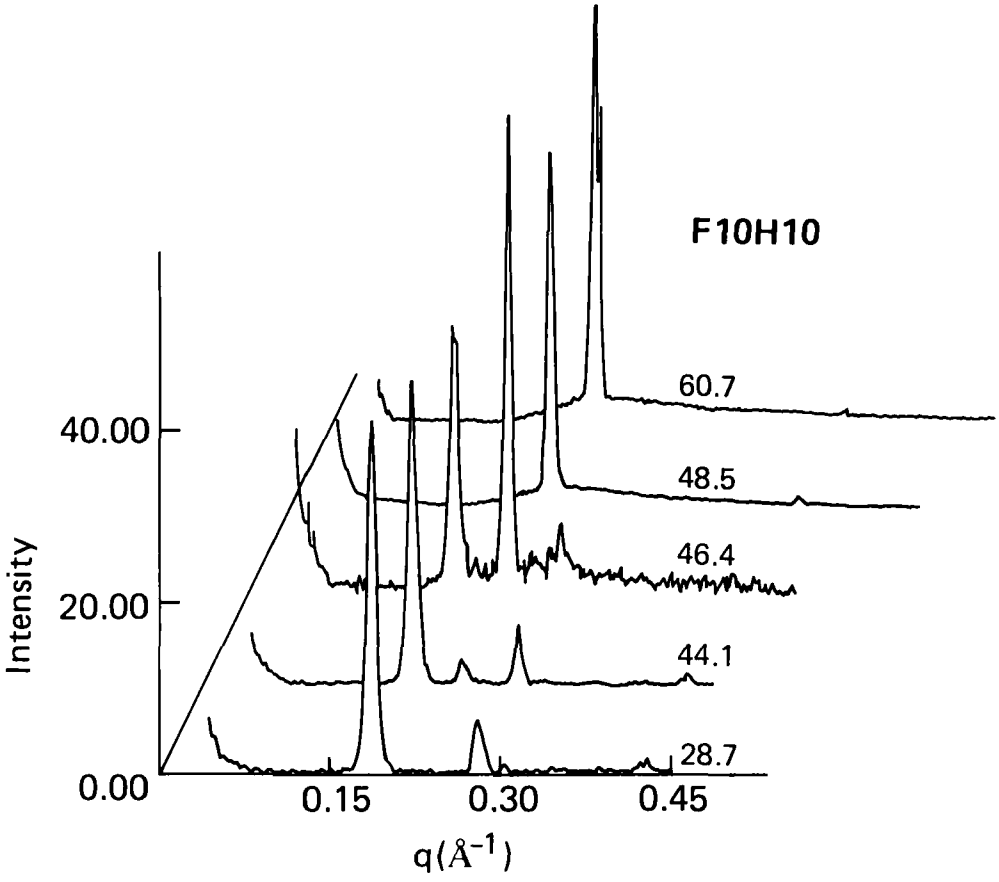

FIGURE 5 SAXS data as a function of the scattering vector q for F10H10 at the indicated temperatures; $q = (4\pi/\lambda)\sin(\epsilon/2)$, where λ is the wavelength (1.429Å) and ϵ is the scattering angle.

between 46.4°C and 48.5°C, where the strong peak associated with a d-spacing of ~34Å disappears. This observation is consistent with scan 1 in Figure 1. From previous work,[1,2] we know that the structure consists of molecules arranged in layers, so that, at all temperatures, the largest d-spacing detected by SAXS can be assigned as representing the layer thickness, *i.e.* the smallest-angle diffraction peak

TABLE II

d-Spacings for F10H10
Data were obtained from as-synthesized material heated to the temperatures indicated.

Temp. °C	Method	Observed d-spacing Å						
20.5	WAXD	22.0	13.2	10.9	7.34	5.46	4.81	4.52
28.7	SAXS	33.87	22.44					
44.1	SAXS	34.33	27.55	22.64	17.69			
46.4	SAXS	34.33	27.43	22.68				
48.5	SAXS	27.49						
50.3	WAXD	13-14	8.9	4.6-4.8				
60.7	SAXS	27.43						

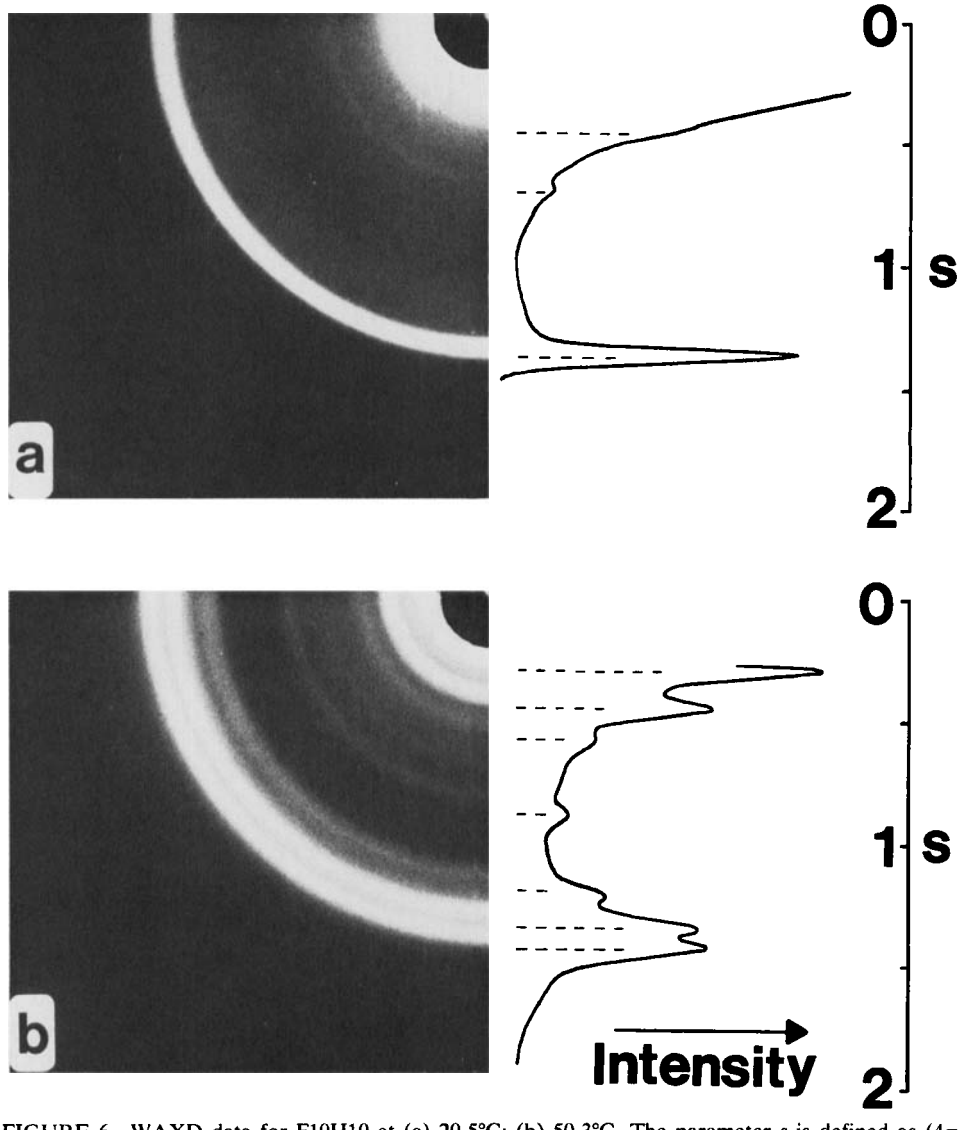

FIGURE 6 WAXD data for F10H10 at (a) 20.5°C; (b) 50.3°C. The parameter s is defined as $(4\pi \sin\theta)/\lambda$, where θ is the angle in Bragg's equation and $\lambda = 1.542$Å.

is indexed as 001. Thus, LC1 is seen to consist of layers which are ~27.4Å thick.

We can postulate the existence of a "void" between adjacent layers, to account for the ability of LC1 to deform under shear, and to allow the individual layers sufficient freedom of relative lateral displacement to explain the absence of *hkl*-type reflections in the diffraction data. The void size must then be greater than the F—F bond distance, which is 1.42Å.[8] Thus we see that the component of layer

thickness which is *not* due to voids is approximately 26.0Å. This is slightly less than the length of a molecule, as will now be demonstrated:

The distance between CF_2 units, measured parallel to the length of the molecules, is 1.3Å.[9] The distance between CH_2 units is taken as 1.25Å.[10] Thus the CF_2—CH_2 bond at the midpoint of the molecule can be assigned a length of 1.27(5)Å. Assuming tetrahedral valence angles, the contribution of the end C—F bond (total length 1.35Å)[11] is 1.10Å, and that of the end C—H bond (total length 1.10Å)[11] is 0.90Å. Molecules therefore have a length approximately equal to

$$(9 \times 1.3) + (9 \times 1.25) + 1.28 + 1.10 + 0.90 = 26.23\text{Å}$$

Since the non-void component of the layer thickness is slightly less than the molecular length, the molecules must be tilted with respect to the layer normal; the angle is $\cos^{-1}(26.0/26.2)$, *i.e.* about 7°.

Because of the limited accuracy of the x-ray data and the molecular length *vs* layer thickness calculation, this argument cannot by itself be regarded as conclusive proof of the existence of so small a tilt. However, it is consistent with the small (~5°) tilt deduced directly from optical microscopy. In the remainder of this discussion, we shall consider our best estimate of the tilt as being the optically determined value of 5°.

The WAXD intensity maximum obtained at 13Å–14Å from LC1 corresponds to 002 or to half the molecular length (measurement of peak position on the original film does not allow these two possibilities to be resolved). The 8.5Å–9.5Å maximum corresponds to 003.

Three maxima in positions similar to those described in the preceding paragraphs have also been identified by x-ray diffractometry.[5]

The broad WAXD maximum centered at ~4.7Å is necessarily intermolecular in origin. We will discuss intermolecular peaks in terms of the antiparallel packing model shown in Figure 7. It is consistent with the packing previously suggested[2] for the related compound F12H12, the single difference being that the model for F10H10 includes the 5° smectic G-like tilt identified and discussed above. The conventional unit cell for this model would be monoclinic (Figure 8a). However, we choose to describe the structure in terms of a triclinic (unconventional) unit cell (Figure 8b), because of the comparative ease with which it will allow us to depict the transition between LC1 and LC2 (Figure 8c). The unit cell can thus be described by the following parameters:

$a = b = r$, a quantity to be determined
$c = 27.5$Å, calculated from the measured layer spacing and the 5° tilt
$\alpha = 90°$, fixed by the model
$\beta = 94.3°$, calculated for a molecular tilt of 5° by using spherical trigonometry
$\gamma = 120°$, fixed by the model.

Given the above model, one would expect the 200, 020 and $\bar{2}20$ reflections to dominate the wide-angle x-ray pattern. A computer program[12] was used to determine the positions of diffraction maxima allowed by the model. When $r = 10.9(2)$Å,

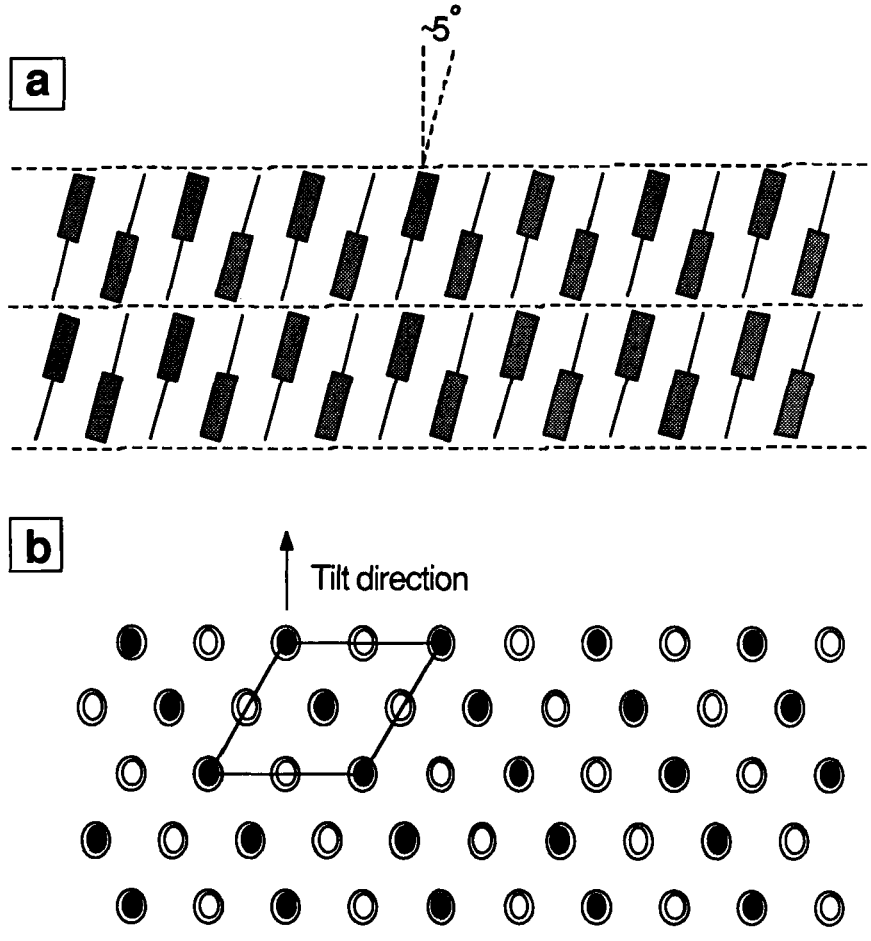

FIGURE 7 (a) Antiparallel packing of molecules proposed for LC1. The structure is viewed in a section that contains the layer normals and a direction of the form [100]. Fluorinated segments are indicated by the "heads", and hydrogenated segments by the "tails". (b) A single layer in LC1, viewed along its normal and sectioned. Fluorinated segments are indicated by the larger ellipses. Hydrogenated segments are denoted by the smaller ellipses; these are filled when the segment lies above the plane of the paper, and empty when the segment lies below.

the calculated spacings for 200, 020 and $\bar{2}20$ are 4.71Å, 4.72Å and 4.72Å respectively, consistent with the single broad WAXD maximum obtained experimentally.

Some justification is necessary for the choice of $\gamma = 120°$ in the model, since the sequence of molecular segments encountered along [110] (only hydrogenated or only fluorinated) is different from that encountered along [100] or [010] (alternating hydrogenated and fluorinated). However, we have already noted that the total length of a fluorinated segment (distance between CF_2 units ~ 1.3Å) is slightly less than that of a hydrogenated segment (distance between CH_2 units ~ 1.25Å). The nearest neighbor distances therefore *all* depend on an interaction between *fluorinated* segments.

From the value of r, we deduce that neighboring molecules are separated by

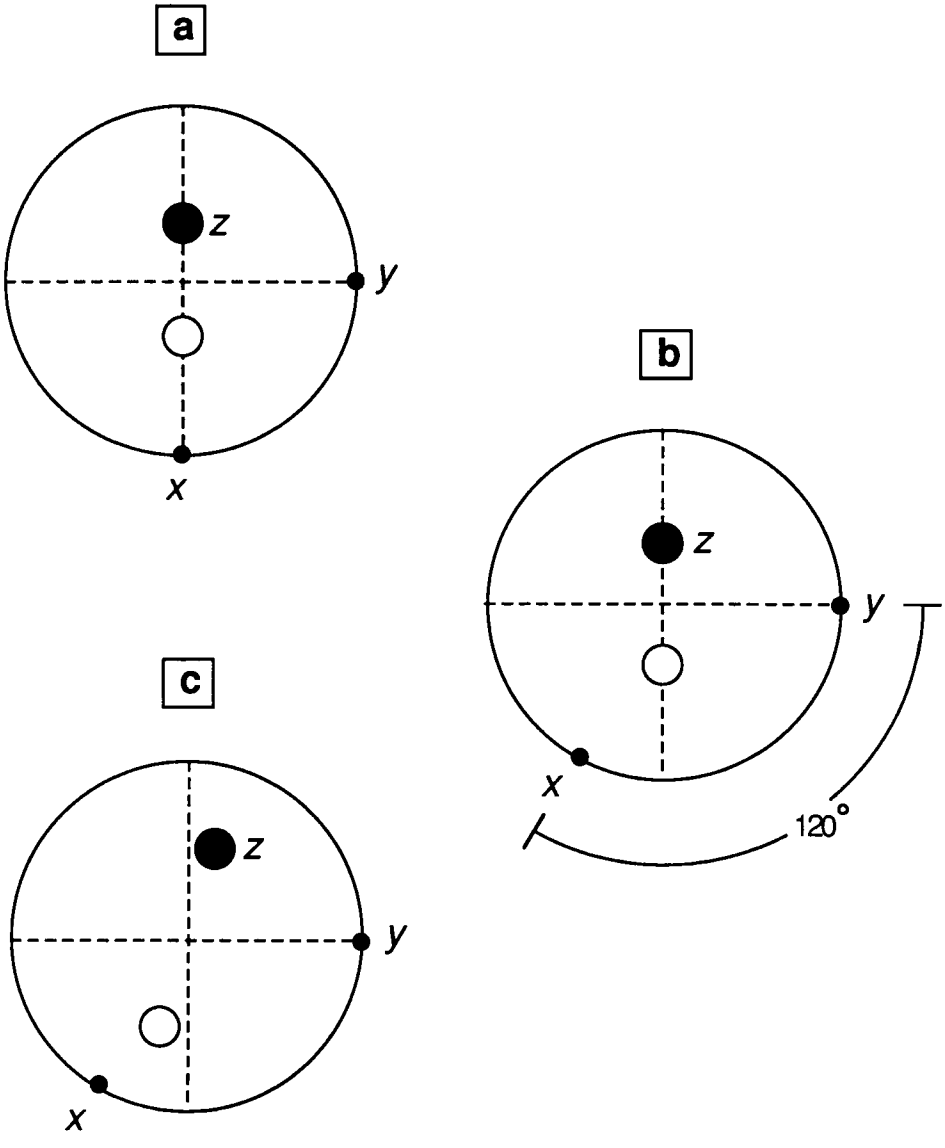

FIGURE 8 (a) Stereographic illustration of monoclinic unit cell for LC1, defining axes x, y and z. (b) More useful triclinic unit cell for LC1. (c) Related triclinic unit cell for LC2.

~5.5Å. This result is comparable with the intermolecular distance of 5.66Å in the structure of poly(tetrafluoroethylene) (PTFE) above room temperature.[13] It is also further evidence that the nearest neighbor approaches in LC1 are limited by interactions between fluorinated segments.

X-ray Diffraction from LC2

Looking next at the SAXS data for LC2, we see that the layer spacing has increased to approximately 34.1Å. This is greater than the total molecular length (~26Å),

but less than three times the length of either the fully hydrogenated or the fully fluorinated segments of the molecule (~39Å). A layer might therefore consist of tilted interdigitated molecules as shown in Figure 9a (for which the tilt angle would be ~30°), or of a tilted bilayer arrangement such as that shown in Figure 9b (requiring a tilt angle of ~50°). The bilayer model has previously been suggested

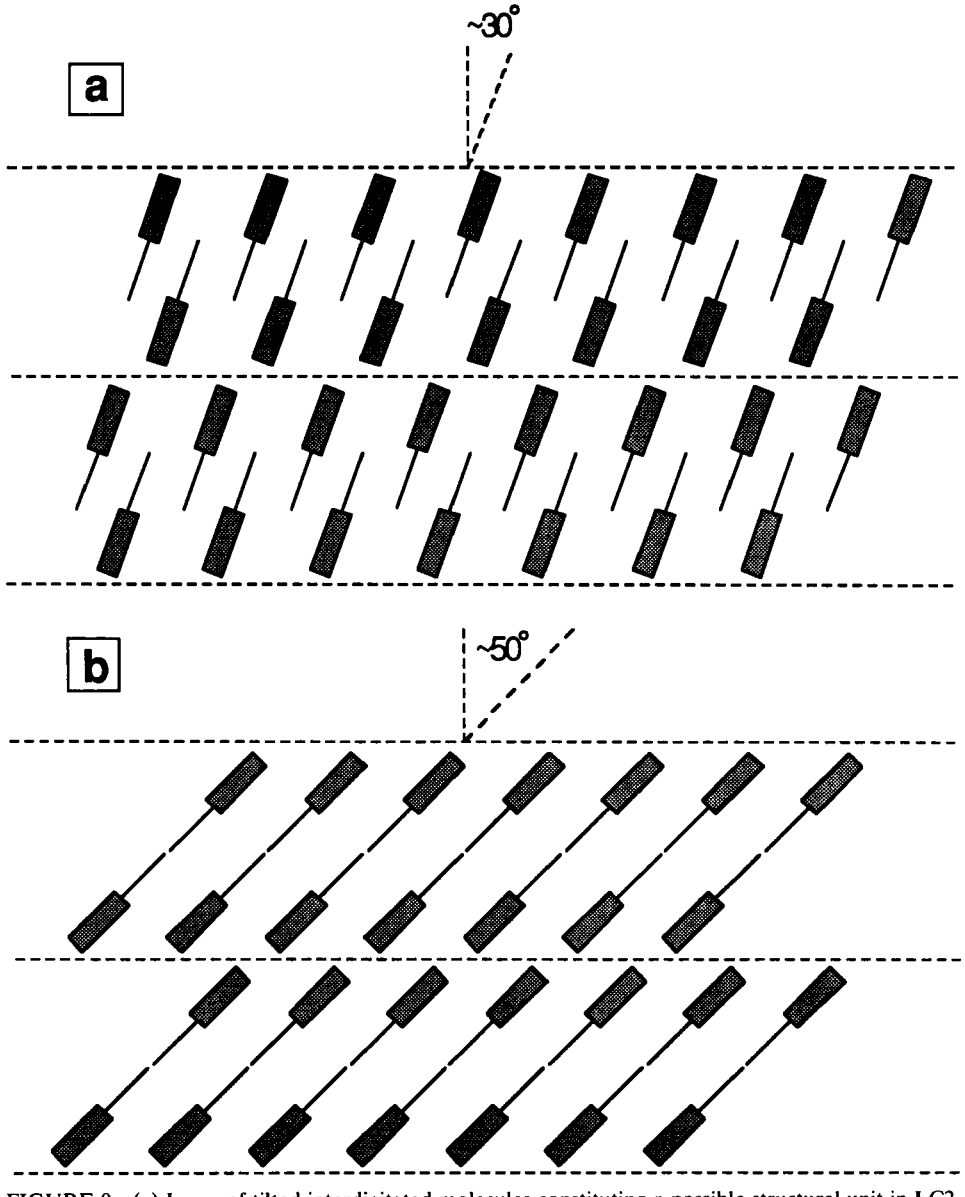

FIGURE 9 (a) Layer of tilted interdigitated molecules constituting a possible structural unit in LC2. (b) Structural unit consisting of a tilted bilayer in LC2. Fluorinated segments are indicated by the "heads", and hydrogenated segments by the "tails". In both cases, the structure is viewed in a section that contains the layer normal and the direction [100].

for F12H12.[2] However, for the present analysis we shall focus on the alternative model, since it requires both a smaller change in tilt and a smaller relative displacement of adjacent molecules to achieve the transformation from LC1.

There are two interdigitated arrangements to choose from. In one, the middle third of each layer (where the closest contacts between molecules occur) would contain only fluorinated segments, and would locally resemble a crystal of PTFE. In the other arrangement, the middle third of each layer would contain only hydrogenated segments, and would locally resemble a crystal of poly(ethylene) (PE). Geometric considerations argue for the latter alternative, since it leaves less space for possible interpenetration of layers.

The reflection at ~17.7Å in the SAXS pattern is identified as 002 (it is obscured by two broader and more intense maxima in the WAXD data). The 003 reflection occurs at ~11.0Å in the WAXD pattern. As was the case for LC1, we can identify a WAXD peak (at ~13Å) that corresponds to approximately half the molecular length, *i.e.* to either a fluorinated or hydrogenated stem.

The peak detected for ~22Å in both the SAXS and WAXD data corresponds to ⅔ of the layer spacing just deduced for LC2, with a slow decrease occurring as the temperature falls. Such a distance would fit the layer spacing for a structure in which the molecules are again tilted by ~30° to the layer normal, but which is similar to LC1 as regards the relative displacement of adjacent molecules. One would then look for a related 002-type reflection at ~11.0Å (coincident with the 003 reflection already described for LC2), and a 003-type reflection would occur at ~7.3Å (which is observed in the WAXD data). One is led, therefore, to consider LC2 as consisting of a *mixture* of two simply related structures. Both are derived from LC1 by an increase in molecular tilt. In one, molecules subsequently undergo a relative longitudinal displacement to form the interdigitated arrangement shown in Figure 9a. The kinetics of this displacement process are likely to be sluggish compared to the change in molecular tilt, providing a ready explanation for the temperature- and time-dependence of the transformation as observed by optical microscopy and DSC.

The relationship between these structures and the observed diffraction patterns is further justification for our neglecting the bilayer model of Figure 9b as an alternative structure for LC2.

The WAXD pattern of LC2 also contains information about intermolecular ordering. However, only three relevant peaks are resolved clearly. Since the two variants of LC2 can be expected to have different sets of lattice parameters within the layers, there are too many variables to allow unambiguous indexing of these peaks.

CONCLUSIONS

1. The compound F10H10 undergoes a reversible liquid crystal–liquid crystal transition.
2. Both liquid crystal phases have a layered structure, and the molecules are

tilted relative to the layer normals. Within each layer, the molecular ordering is pseudo-hexagonal.

3. Above the transition (LC1), the structure is similar to that in smectic G or smectic J. Below the transition (LC2), the tilt can be resolved into a smectic G-like component (towards the midpoint of a hexagon face in the basal plane of the unit cell), and a smectic J-like component (towards a vertex in the basal plane).

4. The transition to LC2 is accomplished in two stages. Firstly, the tilt angle increases. Then adjacent molecules undergo a relative longitudinal displacement, so that all the alkane stems in a given layer become coplanar. The second stage is kinetically disadvantaged relative to the first, and may not occur to completion throughout the specimen.

5. The similar length of the fluorinated and hydrogenated stems leads to many peak overlaps in the x-ray diffraction patterns obtained from F10H10. We are currently making a detailed study of the structural changes accompanying the liquid crystal–liquid crystal transition in related compounds having unequal fluorocarbon and hydrocarbon stem lengths.

Acknowledgments

We are grateful to Drs J. F. Rabolt and B. L. Farmer for edifying discussions, and to Evelyne Hadziioannou and James Ancheta for technical assistance with thermal analysis and photographic processing respectively. We thank IBM United Kingdom for granting a Postdoctoral Fellowship to CV, and IBM Italy for similar support for LED.

References

1. J. F. Rabolt, T. P. Russell and R. J. Twieg, *Macromolecules*, **17**, 2786 (1984).
2. T. P. Russell, J. F. Rabolt, R. J. Twieg, R. L. Siemens and B. L. Farmer, *Macromolecules*, **19**, 1135 (1986).
3. A. M. Levelut, *Journal de Physique*, **37**, C3.51 (1976).
4. J. Doucet, in *The Molecular Physics of Liquid Crystals*, G. R. Luckhurst and G. W. Gray (Eds), Academic Press, London, 1979, Ch. 14.
5. W. Mahler, D. Guillon and A. Skoulios, *Molecular Crystals and Liquid Crystals Letters*, **2**, 111 (1985).
6. G. W. Gray and J. W. Goodby, *Smectic Liquid Crystals*, Leonard Hill, Glasgow, 1984.
7. D. Demus and L. Richter, *Textures of Liquid Crystals*, Verlag Chemie, Weinheim, 1978.
8. CRC *Handbook of Chemistry and Physics*, 64th Edition, CRC Press, Boca Raton, 1983, pg. F-172.
9. B. Heise, H. G. Kilian and F. H. Müller, *Kolloid-Zeitschrift und Zeitschrift für Polymere*, **213**, 12 (1966).
10. This value is obtained from data tabulated for ethane; ref. 8, pg. F-175. See also ref. 11.
11. F. W. Billmeyer, *Textbook of Polymer Science*, John Wiley & Sons, New York, 1984, p. 13.
12. D. K. Smith and M. Holomany, *A FORTRAN IV Program for Calculating X-ray Powder Diffraction Patterns—Version 7*, College of Earth and Mineral Sciences, Department of Geosciences, The Pennsylvania State University, 1980.
13. L. H. Sperling, *Introduction to Physical Polymer Science*, John Wiley & Sons, New York, 1986, pg. 159.